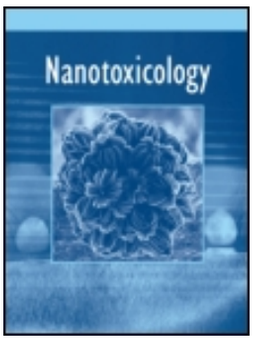

Nanotoxicology

ISSN: 1743-5390 (Print) 1743-5404 (Online) Journal homepage: http://www.tandfonline.com/loi/inan20

Oxidative and molecular interactions of multi-wall carbon nanotubes (MWCNT) in normal and malignant human mesothelial cells

Maricica Pacurari, Xue J. Yin, Min Ding, Steve S. Leonard, Diana Schwegler-berry, Barbara S. Ducatman, Madalina Chirila, Morinobu Endo, Vincent Castranova & Val Vallyathan

To cite this article: Maricica Pacurari, Xue J. Yin, Min Ding, Steve S. Leonard, Diana Schwegler-berry, Barbara S. Ducatman, Madalina Chirila, Morinobu Endo, Vincent Castranova & Val Vallyathan (2008) Oxidative and molecular interactions of multi-wall carbon nanotubes (MWCNT) in normal and malignant human mesothelial cells, Nanotoxicology, 2:3, 155-170, DOI: 10.1080/17435390802318356

To link to this article: https://doi.org/10.1080/17435390802318356

Published online: 10 Jul 2009.

Nanotoxicology, September 2008; 2(3): 155–170

informa
healthcare

Oxidative and molecular interactions of multi-wall carbon nanotubes (MWCNT) in normal and malignant human mesothelial cells

MARICICA PACURARI[1], XUE J. YIN[2], MIN DING[1], STEVE S. LEONARD[1], DIANA SCHWEGLER-BERRY[1], BARBARA S. DUCATMAN[2], MADALINA CHIRILA[1], MORINOBU ENDO[3], VINCENT CASTRANOVA[1], & VAL VALLYATHAN[1]

[1]*Health Effects Laboratory Division, National Institute for Occupational Safety and Health, Morgantown, West Virginia,* [2]*Department of Pathology, School of Medicine, West Virginia University, Morgantown, West Virginia, USA, and* [3]*Faculty of Engineering, Shinshu University, Wakasato, Nagano-shi, Japan*

(Received 13 May 2008; accepted 2 July 2008)

Abstract

Carbon nanotubes are new tools in industry and medicine with their potential applications in many uses. Multiwall carbon nanotubes (MWCNT) with their morphologic similarity to asbestos and wide commercial and biomedical applications necessitate these investigations. The present study investigated the biological reactivity of MWCNT in normal (NM) and malignant (MM) mesothelial cells. MWCNT containing low iron content generated only negligible amounts of reactive oxygen species with both cells. Exposure of both cell types to MWCNT caused cell death, cytotoxicity, DNA damage and apoptosis, which were greater in MM cells. Exposure of both cells to MWCNT caused a parallel activation of two important transcription factors, phosphorylation of H2AX, and PARP activation which were greater in NM cells. Phosphorylation of ERK1/2 and p38 was greater in MM cells than in NM cells. These findings demonstrate that MWCNT are biologically potent activators of molecular events in NM cells associated with mesothelioma development.

Keywords: *Cytotoxicity, DNA damage, mesothelial cells, multi wall carbon nanotubes, reactive oxygen species*

Introduction

Nanotechnology is a rapidly growing field with applications ranging from electronics to biomedical uses including engineered tissues (Craighead & Leong 2000). Engineered carbon nanomaterials, including carbon nanotubes (CNT), have become of great interest due to their unique properties and are expected to produce commercial products worth $2.6 trillion by 2014 (Holman & Lackner 2006). CNT exist mainly in two forms with extensive commercial applications, single-wall (SWCNT) and multi-wall carbon nanotubes (MWCNT). The physicochemical characteristics such as diameter and length differ widely for the two forms of CNT. MWCNT appear more attractive to many applications due to their physical, chemical, thermal, electrical, mechanical, optical properties and their potential to transport materials within the tubes (Endo et al. 2004). SWCNT have a diameter that ranges from 1–2 nm and can be micrometers in length, while the MWCNT used in the present study are 55 nm in diameter with a mean length of 13 microns (Luo et al. 2001; Huo et al. 2003; Maynard et al. 2004). These unique properties may cause undesired biological effects. As CNT are likely to have widespread applications in many fields including consumer and biomedical products, worker/consumer exposure and environmental pollution are likely to occur posing an emerging health concern (Donaldson et al. 2006; Maynard 2007). It has been suggested that inhaled CNT and other nanoparticles are likely to evade phagocytosis, penetrate lung tissue, and translocate to other organs to cause systemic cell toxicity and injury (Oberdörster et al. 2005; Gwinn & Vallyathan 2006; Mercer et al. 2008). Preliminary toxicological studies have shown that intratracheal instillation or pharyngeal aspiration of a SWCNT suspension in rats and mice caused a persistent accumulation of carbon nanotube agglomerates in the lung followed by the rapid pulmonary inflammation and development of fibrotic granulomatous lesions, while more dispersed SWCNT caused progressive interstitial fibrosis (Lam et al. 2004; Warheit et al. 2004; Shvedova et al. 2005). It was also reported that pulmonary

Correspondence: Val Vallyathan, PhD, NIOSH/CDC, 1095 Willowdale Road, Morgantown, WV 26505, USA. Tel: +1 (304) 285 5770. E-mail: vav1@cdc.gov

ISSN 1743-5390 print/ISSN 1743-5404 online
DOI: 10.1080/17435390802318356

exposure to SWCNT provoked cardiovascular effects accompanied by mitochondrial DNA damage of arterial walls and changes in glutathione and protein carbonyl levels promoting atherosclerosis progression of plaques in ApoE-/- mice (Li et al. 2006).

These findings of pulmonary and systemic toxicity are of great concern and suggest that CNT exposure at work during use or when dispersed in the environment could pose an occupational and environmental health hazard. Recently carbon containing nanoparticles including significant fractions of MWCNT have been reported to be present in combustion streams of methane, propane, and natural-gas flames of typical stoves used indoor and outdoor (Bang et al. 2004; Murr et al. 2004a; Lam et al. 2006). Complex nanoparticle aggregates with other common atmospheric pollutants, such as silica and MWCNT, are further confirmed to be present as a major component of fuel-gas combustion in ambient air (Murr et al. 2004b). While SWCNT toxicity has been investigated in a few cellular animal studies, there is a paucity of toxicity studies for MWCNT. Intratracheal instillation of MWCNT in rats resulted in inflammation and pulmonary lesions characterized by the development of collagen-rich granulomas protruding in the bronchial lumen associated with alveolitis (Muller et al. 2005). MWCNT or ground MWCNTs were also biopersistent in the lung at the highest and lowest doses (80% and 40%, of administered dose, respectively) after 60 days. Pulmonary inflammation and fibrosis induced by MWCNT resulted in the overproduction of the inflammatory factor, TNF-α, by macrophages (Muller et al. 2005). The ability of CNT to evade phagocytosis and to penetrate deep into the lung tissue including subpleural areas after pharyngeal aspiration was reported for SWCNT (Mercer et al. 2008). This translocation potential to the pleura combined with the bio-persistent nature and high aspect ratio of CNT could provoke persistent latent interactions with mesothelial cells. The very high aspect ratio of carbon nanotubes along with their physical and toxic properties was suggested to be analogous to other fibrous particles (Maynard et al. 2004). Although the number of studies explored the likely carcinogenic effect of MWCNT due to fibrous-like similarities to crocidolite, a recent study by Takagi et al. (2008) reported the potential of these fibers to be carcinogenic. However, these results have been questioned due to the large dose to which mice were exposed (3 mg/p53+/−mouse) by intraperitoneal administration which resulted in the development of mesothelioma. Another study recently reported asbestos-like fiber-length-depend inflammation of the abdominal wall seven days after intraperitoneal injection of more reasonable doses of MWCNT resulted in inflammation and pathogenic potential in mice (Poland et al. 2008).

The enormous health hazard associated with the use of asbestos fibers in the past highlights the importance of rapidly identifying the potential hazards of engineered CNT with similar morphological and bio-persistent properties. Due to these similarities with crocidolite asbestos (crocidolite), it has been suggested that nanoparticles like CNTs could become the 'asbestos' of the 21st century (Gwinn & Vallyathan 2006). Additional concerns come from studies revealing that particles with nano dimension are markedly more toxic than larger sized particles (Oberdörster, 2001). After years of intense research, it was learned that exposure to asbestos is the primary cause of malignant mesothelioma development in 80–90% of the cases with a long latency.

In light of these early nanotoxicological investigations, and the fact that CNT are fibrous, biopersistent, and may have the ability to translocate to pleura, the present study was undertaken to investigate whether MWCNT in comparison with crocidolite have similar mechanistic effects in normal mesothelial (NM) and malignant human mesothelial (MM) cells. In this study, we used a commercially manufactured MWCNT containing very low levels of metal catalysts (Fe 0.27%), since it is generally conjectured that presence of transition metals is the primary important factor involved in promoting oxidative stress and toxic injury associated with engineered nanomaterials.

In the present study, we investigated the biological reactivity of MWCNT with human mesothelial cells using several molecular biomarkers since the underlying mechanism and complex differences in malignant mesothelioma development is unclear. In order to validate and delineate the specific molecular changes that may be upregulated or downregulated by exposure to MWCNT we used normal malignant mesothelial cells. In addition we also used crocidolite a well documented carcinogen of mesothelioma development as a positive control in some parallel studies. Based on the intrinsic and extrinsic physical-chemical characteristics of asbestos-induced carcinogenicity, several hypotheses have been proposed which include frustrated phagocytosis resulting in enhanced oxidant production and bio-persistent behavior of long fibers. Due to asbestos-like fiber similarities and bio-persistent nature of MWCNT, we investigated several specific parallel or divergent responses of molecular signaling events associated with ROS generation leading to mesothelioma development as reported in studies with asbestos.

Materials and methods

MWCNT

High purity MWCNT produced by the catalytic chemical vapor deposition (CVD) process designed to produce high volume commercialization quantities at low cost was provided as a gift by Bussan Nanotech Research (Mitsui & Co., Ltd., Tsukuba, Ibaraki, Japan). The synthesis of MWCNT was in a vertical tubular reactor reactant system using ferrocene and thiophene as catalyst precursors and carbon feedstock in toluene with hydrogen as the carrier gas. Annealing was done in a graphite-resistance quartz furnace using high purity argon. Decomposition of ferrocene at high temperature between 500–900°C in the presence of iron nanoparticles promoted the breakdown of volatile carbon compounds to produce metastable carbides, allowing the carbon to diffuse through iron nanoparticle rapidly to form the carbon precipitates. They are self-assembled into a bundle of rope structures. Detailed manufacturing and annealing conditions have been described previously (Kim et al. 2005; Chen et al. 2007). The MWCNT were heated to 2800°C in an argon atmosphere using a graphite furnace to improve structural integrity and to remove polyaromatic hydrocarbons and a significant amount of iron. Iron content measured by atomic absorption spectroscopy after purification ranged from 0.26–0.34%. Other potentially toxic metals detected in quantitation limits are presented in weight percentage ($\geq$0.01%) in Table I. Length and diameter of the MWCNT samples used in this study were determined orphometric analysis of several electron micrographs visualized using microscopic images magnified at 2000 $\times$ using an image capturing system (Olympus AX 70 and SamplePCI, Compix, Cranberry Township, PA, USA). Fiber length and diameter were digitized from 110 images using an automated image digitizer (Optimas 6.51, Media Cybernetics Inc., Silver Spring, MD, USA). These measurements showed the average length of fibers to be 8.19 μm with a diameter of 81 nm. The specific average surface area was 26 m^2/g as measured by the Brunauer-Emmett-Teller (BET) nitrogen adsorption method (Brunauer et al. 1938).

For cell culture studies, MWCNT stock (5 mg/ml) was prepared by an indirect ultrasonication dispersion process at 4°C using full power for 10 min in RPMI-1640 medium containing 1% fetal bovine serum (FBS) (American Type Culture Collection, Rockville, MD, USA).

This was followed by a brief direct probe ultrasonication at 10% output for 1 min in RPMI containing 1% FBS. Samples that were used for cellular studies were freshly prepared from the stock on the day of cell treatments to desired concentrations of MWCNT in RPMI containing 0.1% FBS and resonicated by a direct ultrasonication for 1 min before use.

Raman spectroscopy

Dispersed MWCNT (2.5 mg/ml in PBS) were placed on a 9-mm diameter silicone stub glued to a glass microscope slide. The sample was placed under the laser beam and excited in a Raman spectroscope. Spectra were collected in back-scattering geometry using a 514.5 nm argon ion laser. A confocal microscope with an 80 $\times$ magnification objective was used to focus the laser beam and to collect the scattered light. The laser power was 16 mW at the sample, and the beam was focused to 5 μm diameter spot size giving a laser power density was 2 W/cm^2. Five randomly selected spots on the sample were analyzed to collect one Raman spectrum from each sample and a representative spectrum from one of the spots is presented in Figure 1.

Light microscopy and transmission electron microscopy (TEM) of MWCNT

The MWCNT prepared as described above were diluted in deionized water, applied on slides, and observed under a light microscope. For TEM, the samples prepared as above in 0.1% FBS were diluted and then deposited on a formvar-coated copper grid, dried, and photographed using a JEOL-1220 transmission electron microscope. A large number of discrete nanotubes and few agglomerates of MWCNT were present.

Determination of trace metal content in MWCNT

The metal content of the MWCNT sample used in the present study was determined by inductively coupled plasma-atomic emission spectroscopy (ICP-AES). Weighed amounts of samples were digested in 1 ml of concentrated HNO_3 and 5 ml

Table I. Physical and chemical characteristics of MWCNT.

	Carbon purity	Mean diameter	Mean length	Surface area
MWCNT as used in exposure to cells	99.5%	81 $\pm$ 5 nm	8.19 $\pm$ 1.7 μm	26 m^2/g (Range 24–28)
Toxic metals	Al	C	Fe	Zn
ICP-AES%	0.035	0.017	0.27	0.009

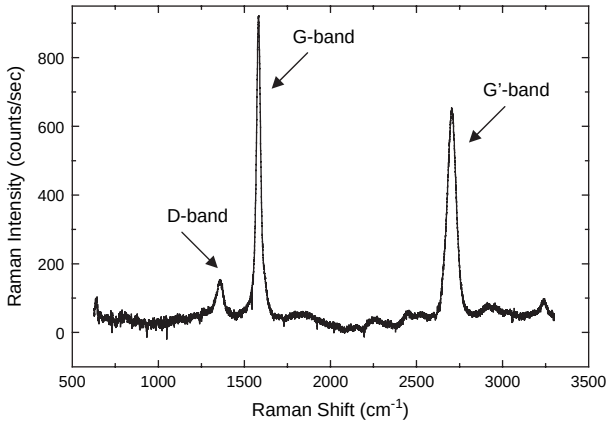

Figure 1. Representative Raman spectrum from MWCNT obtained with 514.5 nm laser. A small disorder D band at 1350 cm^{-1}, a graphite G band at 1580 $cm^{-1}$and a G-band (second order of D-band) at 2700 cm^{-1} were present in all spot analyses.

$HClO_4$ at 150°C. An additional 5 ml $HClO_4$ was added and the reagent refluxed for 15 days at 180°C. The digested samples were dried at 150°C and the residue was then dissolved in 10 ml 4% HNO_3 and 1% $HClO_4$ for trace metal analysis and transferred to volumetric flasks, diluted to a final volume of 25 ml with ASTM Type II water. Aliquots of the digestate were then analyzed for 31 elements and metals using a Thermo-Jarrel Ash ICAP-61 inductively coupled plasma emission spectrometer controlled by Thermospec software, according to NIOSH method 7300 (NMAM 1994). Concentrations of toxic trace metals and other physical chemical characteristics of MWCNT and crocidolite are presented in Table I. Metals reported in MWCNT are in the detectable limits of quantitation (Table I).

Cell lines and cell culture

NM and MM cell lines were obtained from American Type Culture Collection (Rockville, MD, USA). Cells were grown in RPMI-1640 medium (American Type Culture Collection), supplemented with 100 μg/ml streptomycin, 100 units/ml penicillin, and 5% FBS at 37°C in a humidified atmosphere (5% CO_2 plus 95% air). The medium was changed twice weekly, and cells were trypsinized and subcloned weekly. Prior to particle treatment, the culture medium was replaced with the RPMI-1640 medium containing100 μg/ml streptomycin, 100 units/ml penicillin, and 0.1% FBS.

Electron spin resonance (ESR) assay

The production of reactive oxygen species (ROS) following treatment with MWCNT was determined using an EMX spectrometer (Bruker Instruments, Billerica, MA, USA) and a flat cell assembly, as described previously (Leonard et al 2003). The spin trap, 5, 5-dimethyl-1-pyrroline-1-oxide (DMPO), was purified by charcoal decolorization and vacuum distillation. The DMPO solution, thus purified, did not contain any ESR detectable impurities. The phosphate buffer (pH 7.4) was treated with Chelex 100 to remove transition metal ion contaminants. Reactants were mixed in test tubes in a final volume of 1.0 ml. The reaction mixture was then transferred to a flat cell for ESR measurement. Experiments were performed at room temperature and under ambient air.

Cell viability using trypan blue exclusion assay

The NM and MM cells (1×10^5) were seeded overnight in normal growth medium. After 12 h, the cells were exposed to 12.5, 25, 50, 125 μg/cm^2 of MWCNT or crocidolite in the same mass concentrations in 0.1% FBS or vehicle alone for 24 h. After the incubation period, the cells were washed in Hank's buffered salt solution (HBSS), harvested with a cell scraper in HBSS, and placed on ice. Cell viability was determined by light microscopy immediately after the exposure using trypan blue stain and hematocytometer (Sigma Aldrich Co., St Louis, MO, USA). The results are expressed as percent of viable cells.

Cytotoxicity assays

The NM and MM cells (10^6), seeded in 6-well plates overnight, were treated with 5, 25, 50, 100 μg/cm^2 of MWCNT, crocidolite, or vehicle alone for 24 h. Lactate dehydrogenase (LDH) activity, an indicator of cellular cytotoxicity, was determined in the culture supernatants.

Measurements were performed with an automated Cobas Fara II analyzer (Roche Diagnostic System, Montclair, NJ, USA). The LDH activity, expressed as units per liter of culture medium, was determined by measuring the formation of reduced nicotinamide adenine dinucleotide using the Roche Diagnostic reagents and procedures (Roche Diagnostic Systems, Indianapolis, IN).

Apoptosis assay

The NM and MM cells (10^4), seeded in 96-well plates overnight, were treated with 25, 50 μg/cm^2 of MWCNT, or vehicle alone for 24 h. Apoptosis was measured using the Cell Death Detection ELISA Plus Kit (Roche Diagnostics Systems, Indianapolis, IN, USA) per manufacturer's instructions. In brief, cell lysates were incubated in anti-histone-coated microtiter plates. DNA attached to the bound

histones was detected with peroxidase-conjugated anti-DNA antibody. After washing steps, substrate was added to the microtiter wells and color change was read at 405 nm by a SpectraMax 250 microplate spectrophotometer reader (Roche Diagnostics, Montclair, NJ, USA).

DNA damage by Comet assay

The NM and MM cells (10^6), seeded in 6-well plates overnight, were treated with 25, 50 μg/cm^2 of MWCNT, or vehicle alone for 24 h. Comet assay was carried out using a commercially available Comet Assay kit (Trevigen, Gaitherburg, MD, USA), according to the manufacturer's instructions. Briefly, slides with agarose-embedded cells were immersed in prechilled lysing solution and kept at 4°C for 1 h. The slides were then placed in a horizontal gel-electrophoresis tank, covered with cold alkaline electrophoresis buffer (300 mM NaOH, 1 mM EDTA, pH > 13) for 20 min and electrophoresed at 300 mA for 30 min. After electrophoresis, the slides were fixed with 70% ethanol, dried, and stained with SYBR Green I. All the above steps were conducted under very dim light or dark to prevent potential DNA damage by light. The slides were visualized using fluorescence microscopy, with an image capturing system (Olympus AX 70 and SamplePCI, Compix, Cranberry Township, PA, USA). For each sample a minimum of 50 cells were scored at 400 × magnification. The lengths of the comet tail, which indicate DNA damage resulting in the migration of tail, were digitized as the distance between edge of head and end of tail using an automated image analysis system (Optimas 6.51, Media Cybernetics Inc., Silver Spring, MD, USA).

Measurement of H2AX phosphorylation

H2AX phosphorylation was measured using a commercially available chemiluminescence assay and by immunofluorescence microscopy with mouse monoclonal anti-phospho-H2AX (Ser 139) (Upstate, Temecula, CA, USA). NM and MM cells cultured in black-wall/clear bottom microplates were exposed to SWCNT or crocidolite for 24 h. Detection of H2AX phosphorylation was determined according to manufacturer's protocol (Upstate, Temecula, CA, USA). Briefly, after fixation and permealization of cells, phosphorylated histone H2AX is detected by the sequential addition of anti-phospho-H2AX and an anti-mouse-HRP conjugate. The chemiluminescent HRP substrate LumiGLO is then added, and the signal is measured using a microplate luminometer. For immunofluorescence microscopy, the cells were seeded onto sterile glass cover slips, placed in 12-well plates, and exposed to 25, 50 μg/ml of MWCNT or crocidolite for 24 h. After the treatments, the cells were washed once with TBS, fixed in 95% ethanol 5% acetic acid for 5 min at room temperature. The cells were washed three times with PBS, and then blocked in 3% BSA/TBS for 1h at room temperature. For immunodetection, the cells were incubated with 2 μg/ml anti-phospho-Histone H2AX (Ser 139) in blocking buffer overnight at 4°C. Cells then were washed three times with TBS for 5 min, and incubated with secondary goat anti-mouse FITC or goat-anti-mouse Alexa 594 antibody (Molecular Probes, Eugene, OR, USA) in the dark for 1 h at room temperature. Following incubation, the cells were washed five times with TBS, mounted with ProlongLife DAPI mounting media, and images were acquired using Carl Zeiss LSM 510 (Carl Zeiss Inc., Thornwood, NY, USA) laser scanning microscope. Activation of H2AX (Ser 139) results in focal concentrations of phosphorylated H2AX that can be detected by microscopy, and these focal concentrations are termed γH2AX foci.

Western blot analysis of cleaved PARP

NM and MM cells were subcultured in 6-well plates and maintained for 24 h in 10% FBS RPMI 1640 growth medium. The standard growth medium was then replaced with 0.1% FBS containing medium and the cells were exposed to 50 μg/cm^2 MWCNT or crocidolite for 0, 6, and 18 h. After exposure, the cells were washed once with two volumes of ice cold 1 × PBS, and lysed with 1 × SDS sample blue buffer supplemented with 1 μl/ml Sigma's Protease inhibitor cocktail™ in 1 mM PMSF on ice for 10 min. Cell debris was removed by microcentrifugation for 15 min at 14,000 rpm. Twenty μg protein per sample were separated on 10% SDS-PAGE gels and transferred to nitrocellulose membranes. Immunoblotting for cleaved PARP, full PARP, and Beta-actin was determined using the same membrane after stripping of the blot. The optical densities of bands were analyzed using a BioRad Fluor-S™ MultiImager gel documentation system. Individual band intensities for cleaved PARP were expressed as fold activation after normalizing the intensities to Beta-actin and full PARP.

Protein kinase phosphorylation assay

The NM and MM cells (106), seeded in 6-well plates overnight, were treated with 25 μg/cm^2 of MWCNT or vehicle alone for 0, 5, 15, 30, 60, or 120 min. After each treatment, the cells were lysed in a lysing buffer (Tris-Glycin SDS sample buffer,

Invitrogen, Carlsbad, CA, USA), supplemented with 50 mM DTT and left on ice for 10 min. Whole cell lysates were collected and sonicated for 8 sec, boiled at 100°C for 5 min, and centrifuged at 5500 rpm at 4°C. Protein contents in the supernatants were determined using a BCA Protein Assay Kit (Pierce, Rockford, IL, USA). Immunoblots for phosphorylation of ERKs, JNKs, and p38 kinase were carried out using PhosphoPlus MAPK antibody kits as described in the protocol of New England BioLabs (Boston, MA, USA). Phosphospecific antibodies were used to detect phosphorylated sites of ERKs, JNKs, and p38 kinase as previously described. Nonphosphospecific antibody against p38 kinase protein was used to ensure equal loading of protein and normalize the phosphorylation assay by using the same transferred membrane blot following a stripping procedure.

Activation of AP-1 and NF-κB

The NM and MM cells (10^6), seeded in 6-well plates overnight, were treated with 25 μg/cm^2 of MWCNT or vehicle alone for 1, 2, or 4 h. Nuclear extractions were prepared using a nuclear extraction kit (Panomics Inc., Redwood City, CA, USA), and activation of AP-1 and NF-κB was determined using respective ELISA kits (Panomics Inc.) according to the manufacturer's instructions.

Statistics

The results are presented as means ± SEM of three experiments, and statistical analyses were performed by Student's *t*-test or one-way ANOVA. The statistical significance of differences was set at $p < 0.05$.

Results

Raman spectroscopic analysis

A representative Raman spectrum is presented to illustrate the bands in MWCNT sample analysis showing the D-, G-, and G′- bands (Figure 1). In all five spot analyses of Raman spectra obtained, three main bands specific to CNT were identified: The D-band (disorder band, associated with vibrations of amorphous carbon, impurities and defects); the G-band (graphite band, present in all carbon-based materials), and G′-band (second order of D-band) are present. The calculated R value ranged between 0.060–0.118 with an average of 0.103. The R value is defined as the ratio between the absolute intensity of D-band and G-bands. This small R value is considered characteristic of high-purity MWCNT (Koyama et al. 2006).

Chemical and physical analysis of MWCNT

MWCNT are neither water soluble nor wettable and are therefore extremely difficult to disperse. To generate a more homogenous dispersion, MWCNT were ultrasonicated by indirect sonication for 10 min followed by direct sonication for 1 min in RPMI-1640 medium supplemented with 0.1% FBS as dispersion vehicle. Light microscopic examination showed that the procedure resulted in a production of a mixture of MWCNT structures containing predominantly long loosely associated MWCNT strands as well as small amounts of agglomerated mat structures (Figure 2A). In Figure 2B, an inset from Figure 2A is shown at a higher magnification. Scanning and transmission electron microscopic studies showed the MWCNT samples contained predominately loosely associated long fibers (Figure 2C, 2D). From electronmicroscopic images fiber length and diameters measured by digitized image measurements showed that the average length to be 8.19 ± 1.71 μm and an average diameter of 81 ± 5 nm. The frequency distribution of fibers longer than 5 μm was 60% and fibers shorter than 5 μm in length were 40%. Results of these measurements are presented in Figure 2. Surface area of MWCNT ranged from 24–28 m^2/g with an average of 26 m^2/g.

The MWCNT samples were analyzed for metal contamination. Among the metals analyzed by ICP-AES only Al, Cr, Fe, and Zn were found in measurable limits of quantitation in MWCNT samples analyzed. The physical and chemical characteristics of MWCNT are presented in Table I.

ROS generation

Induction of oxidative stress by unpurified SWCNT in other cells such as HaCaT cells (human keratinocytes) has been reported, and as a consequence of oxidant stress significant cell death has been observed (Shvedova et al. 2003; Manna et al. 2005). To study the induction of oxidative stress by MWCNT in NM and MM cells, the cells were exposed to the particles and generation of ROS was monitored using ESR studies. When NM and MM cells exposed to MWCNT a very small increase in the levels of ROS were detected (Figure 3A, 3B). The ESR spectrum consists of a 1:2:2:1 quartet with hyperfine splittings of $a_H = a_N = 14.9$ G, where a_H and a_N denote splittings of the nitroxyl nitrogens and α-hydrogen, respectively. Based on these splittings and the 1:2:2:1 line shape, the spectrum was assigned the DMPO-$^{\bullet}$OH adduct, which is evidence of hydroxyl radical ($^{\bullet}$OH) generation. This limited generation of ROS in the absence of appreciable amounts redox active metals could be considered as resulting from phagocytosis of the particles. This is

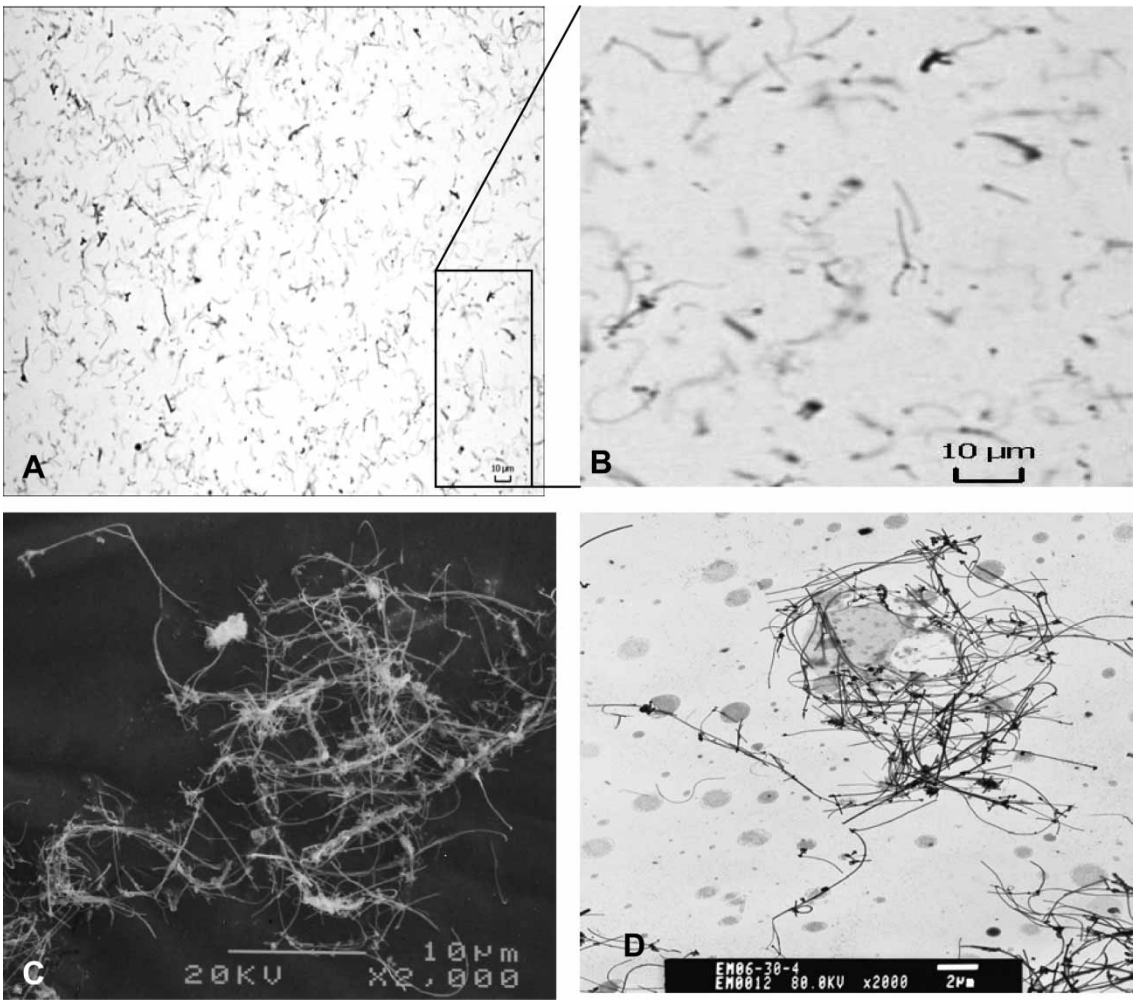

Figure 2. Microscopic images of MWCNT samples prepared in 0.1% FBS that were used in cellular studies. (A) Light micrograph of a random sample of MWCNT prepared for cellular studies in cell culture medium containing 0.1% FBS. (B) An inset of boxed area is shown at a higher magnification. (C) Scanning electron micrograph of MWCNT transferred to a double sided tape and coated with gold/palladium. (D) Transmission electron micrograph of MWCNT sample. Single MWCNT fibers and impurities are visible.

apparent from the lack of significant inhibition with deferoxamine.

Cell death and toxicity

The effect of MWCNT on cytotoxicity in NM and MM cells was first evaluated by determining LDH release from the MWCNT-treated cells. Treatment of these cells with MWCNT resulted in a concentration-dependent increase in the release of LDH compared with control (Figure 4), as well as a significant decrease in the viability of both NM and HM cells (Figure 5). To further assess the extent of cellular damage by MWCNT particles, programmed cell death was determined by apoptosis assay in NM and MM cells. The results show that treatment with MWCNT led to a significant increase in apoptosis in both cell types. However, the apoptosis was higher in MM cells, suggestive of a cell-specific neoplastic cellular response (Figure 6). In addition, DNA damage, as detected by the comet assay in NM and MM cells treated with MWCNT, showed a dose-dependent damage in both cell types. The results also showed that the DNA damage was significantly greater in MM cells compared to NM cells (Figure 7A, 7B).

H2AX phosphrylation

In the present study, we investigated whether MWCNT in comparison with crocidolite induce the activation of histone H2AX using ELISA, and immunoflourescence microscopy. H2AX is rapidly phosphorylated at Ser 139 following treatments that induce DNA double-strand breaks (DBSs) (Cowell et al. 2007). Exposure of NM and MM cells to 12.5 and 25 µg/ml MWCNT resulted in a significant increase in phosphorylation of H2AX on Ser-139, which was moderately more in NM cells. Same concentrations of crocidolite induced a significantly

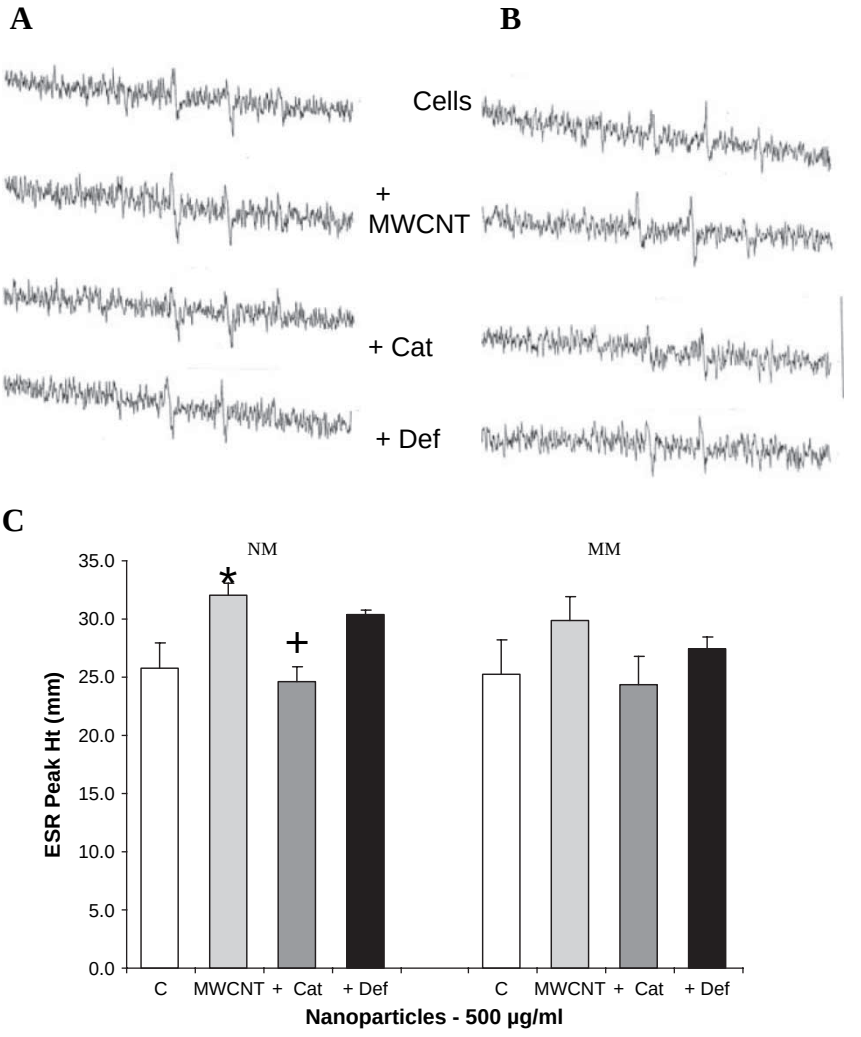

Figure 3. Generation of ROS from control, MWCNT-treated NM, and MM cells. ESR spectra of (A) normal mesothelial cells, and (B) malignant mesothelial cells (10^6 /ml) incubated in a medium containing 100 mM DMPO, PBS, and with or without 500 µg/ml MWCNT for 10 min at 37°C. (C) Semi-quantitative analysis of ESR spectra from 500 µg/ml MWCNT-treated NM, and MM cells. Co-incubation with catalase (2000 units/ml) and deforaxamine (2 mM) were used to confirm the generation of $^{\bullet}$OH radicals and investigate the role of Fe in ROS generation. Instrumental conditions: microwave power, 63.96 mW; modulation amplitude, 1.0 G; time constant, 40.96 ms; center field, 3480 G; sweep width, 100 G. The results presented are the means ± SEM of three experiments. *Indicates a significant increase from control ($p < 0.05$). +Indicates a significant decrease by catalase ($p < 0.05$).

greater phosphorylation in both cell types (Figure 8C). Immunofluorescence microscopic analysis indicated the induction of distinct foci following NM and MM cells exposure to 25 or 50 µg/ml MWCNT. Similar concentrations of crocidolite resulted in more distinct foci formation in both cells types (Figure 8A, 8B). The formation of γH2AX foci was higher in NM cells compared to MM cells (Figure 8A, 8B).

Activation of Poly(ADP-ribose) polymerase (PARP)

We investigated the effects of exposure to MWCNT or crocidolite in NM and MM cells on the activation of PARP. PARP is a chromatin-bound enzyme activated by DNA strand breaks which may alter the chromosomal proteins to facilitate DNA repair. Our studies with MWCNT and crocidolite show time dependent activation of cleaved PARP in NM cells. Crocidolite and MWCNT induced significantly greater activation of PARP in NM cells compared to MM cells. In MM cells there was a moderate activation of cleaved PARP after 18 h by MWCNT as well as crocidolite (Figure 9).

Activation of AP-1 and NF-κB

Transcription factors, AP-1 and NF-κB, both play important roles in carcinogenesis (Ding et al. 1999). Therefore, we investigated the effects of MWCNT on AP-1 and NF-κB activation in mesothelial cells. The results show that treatment with MWCNT

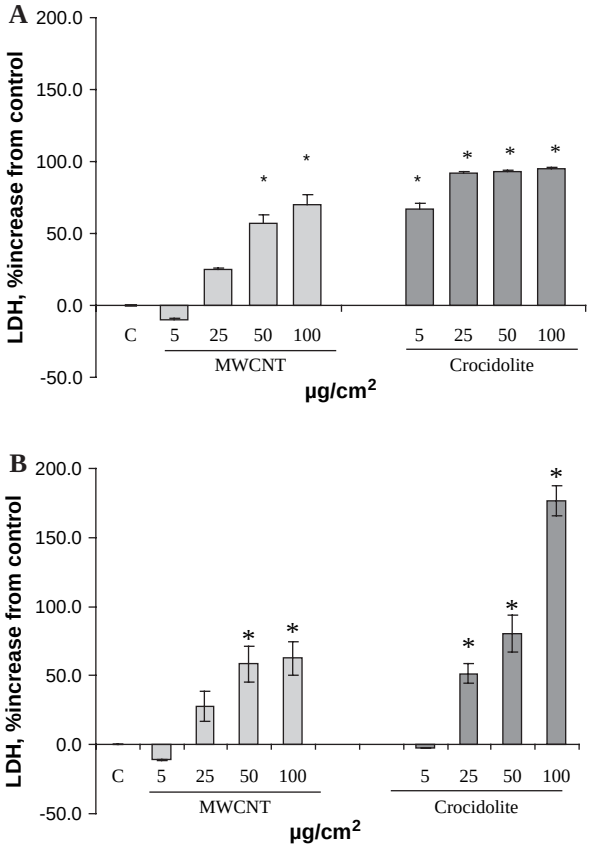

Figure 4. Dose-dependent effect of MWCNT on the release of LDH from (A) NM and (B) MM cells. The cells were treated with dispersion vehicle (control), 5, 25, 50, and 100 μg/cm^2 MWCNT or crocidolite for 24 h and LDH activity in culture supernatants was measured as described in *Materials and methods*. Results are presented as mean ± SEM of three experiments. *Significantly different compared to control ($p \leq 0.05$).

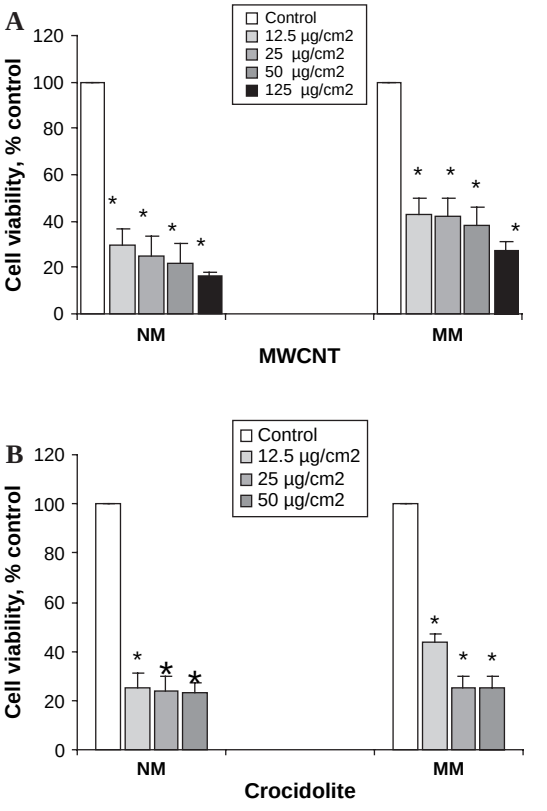

Figure 5. Effect of MWCNT and crocidolite on the viability of NM and MM cells. (A) MWCNT effect on NM and MM cells viability. (B) Crocidolite effect on NM and MM cells viability. The cells were treated with dispersion vehicle (control), 12.5, 25, 50, and 125 μg/cm^2 MWNT, or crocidolite for 24 h, and cell viability was determined by trypan blue exclusion assay as described in *Materials and methods*. *Significant decrease from control ($p < 0.05$).

resulted in a significant activation of AP-1 and NF-κB in NM cells (Figure 10A, 10B). Both transcription factors showed a decline after 4 h in NM cells. A significantly increased activation of AP-1 and NF-κB in NM cells was evident with 25 μg/cm^2 in one hour. On the other hand, in MM cells a longer time exposure (4 h) to same dose of MWCNT induced only a moderate activation of NF-κB (Figure 10B).

MAPKs activation

Since mitogen-activated protein kinases, including p38, ERK1/2, and JNKs, are involved in the activation these transcription factors, we explored the activation of all these kinases. MAPKs are the upstream kinases responsible for *c-Jun* phosphorylation and AP-1 and NF-κB activation; we next tested which class of MAPK is involved in the induction of AP-1 and NF-κB activation by MWCNT. NM cells exposed to MWCNT did not activate ERK over the examined time points (Figure 11B), while after 60 and 120 min p38 induced a 3.8-fold activation (Figure 11C). However, treatment of MM cells with MWCNT led to an increased induction of ERK1/2 and p38 phosphorylation that peaked after

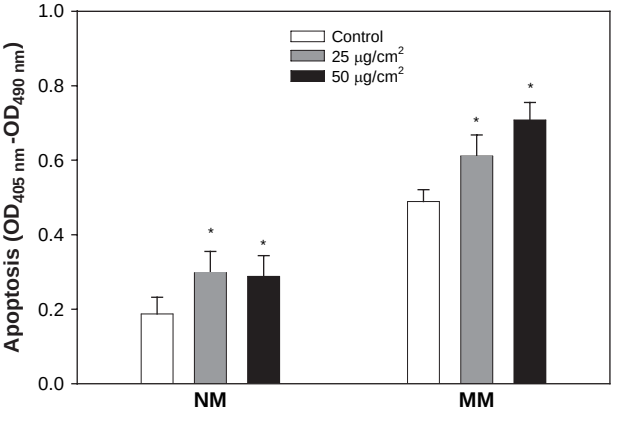

Figure 6. Effect of MWCNT on apoptosis of NM and MM cells. The cells were treated with dispersion vehicle (control), 25, or 50 μg/cm^2 MWNT for 24 h. Apoptosis was determined by ELISA. *Significant increase from control ($p < 0.05$).

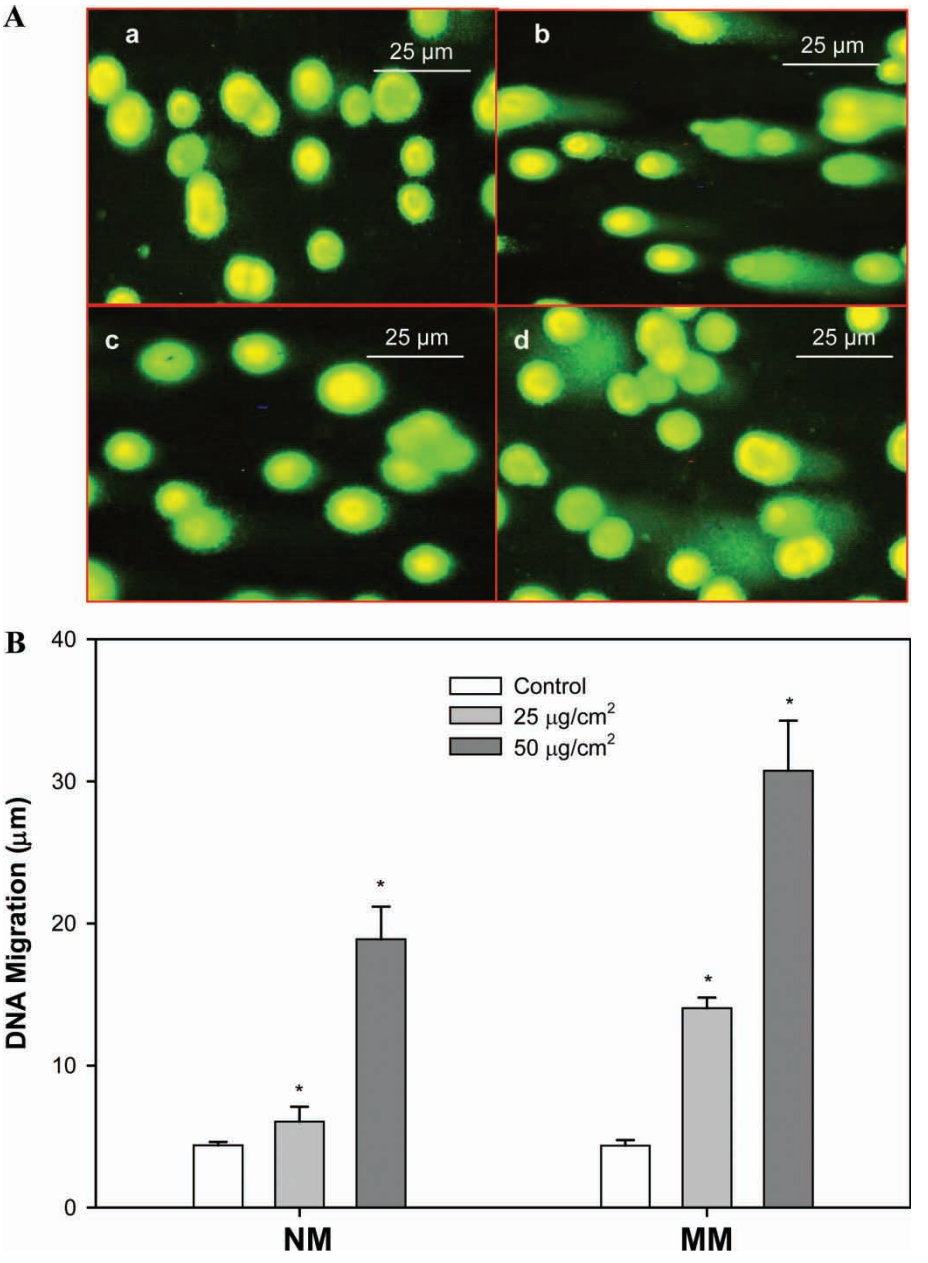

Figure 7. Effect of MWCNT on DNA migration in NM and MM cells using the comet assay. (A) Micrographs of NM and MM cells treated with dispersion vehicle (control), 25, or 50 µg/cm^2 of MWNT for 24 h: a = control NM cells, b = MWCNT (50 µg/cm^2)-treated NM cells, c = control MM cells, d = MWCNT (50 µg/cm^2)-treated MM cells. Comets were visualized using fluorescence microscopy with an image capturing system. (B) Semiquantitative anlysis of concentration-dependent effects of MWCNT on DNA migration in NM and MM cells. The length of comet tail from digitized images was quantitated as described in *Materials and methods*. Fifty cells were scored for each sample. *Indicates a significant increase from control ($p < 0.05$).

15 min of stimulation (Figure 11). Phosphorylation of JNKs examined in NM and MM cells using similar MWCNT mass exposure times did not cause an increase (data not shown).

Discussion

Carbon nanotubes have been the focus of many scientific studies due to their enormous potential applications in multiple industrial and biomedical fields. SWCNT chemically functionalized have been shown to enter fibroblast, promyelotic leukemia (HL60) cells and T cells (Kam et al. 2004; Pantarotto et al. 2004). However, there is limited information on the potential interactions of MWCNT with mesothelial cells and the resultant toxicologic and molecular changes. MWCNT have the ability to form micrometer-sized particles that can be fibrous or rod-shaped. The diameter ranges from 0.01–0.2 micrometer and the length can be of

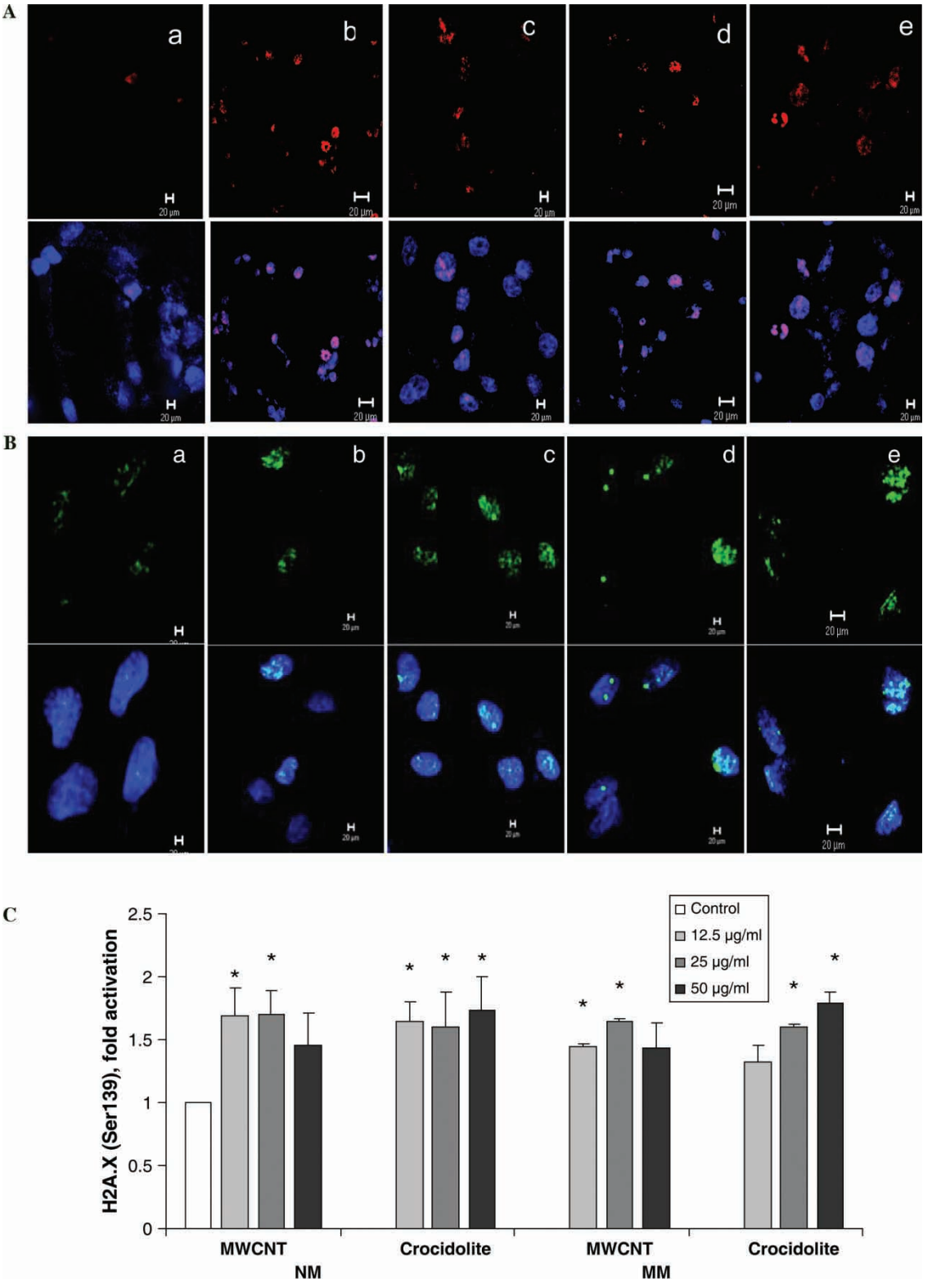

Figure 8. Effect of MWCNT and crocidolite on the activation of γ-H2AX (Ser 139). (A) Induction of γ-H2A.X nuclear foci by MWCNT and crocidolite in (A) NM and (B) MM cells. The cells were exposed to 25, 50 µg/ml MWCNT or crocidolite for 24 h. After the exposure, the cells were prepared as described in *Materials and methods*, and then stained for γ-H2AX (green and red) or DNA (blue). a: control, b-c: MWCNT, d–e: crocidolite. (C) Activation of γ-H2AX in NM and MM cells determined by ELISA. The assay was performed according to manufacturer's protocol as stated in Materials and Methods. The absorbance values were normalized to control values. The data is presented as mean ± SEM of three experiments. *Significantly different compared to control ($p < 0.05$).

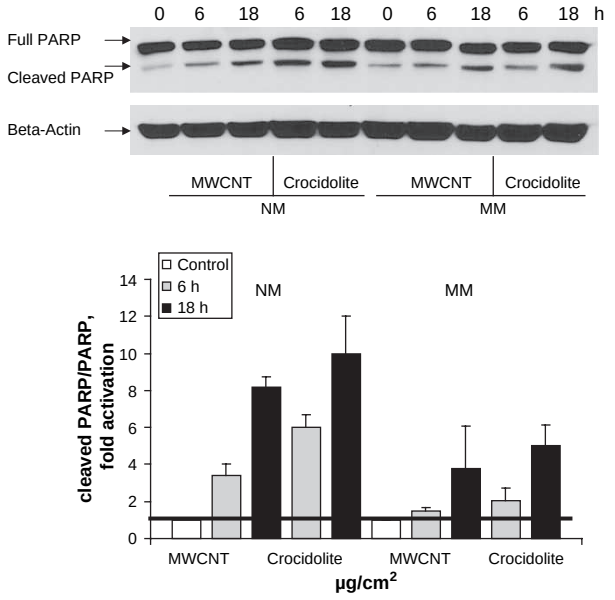

Figure 9. Effect of MWCNT and crocidolite on the activation of PARP in NM and MM cells. Normal and malignant mesothelial cells were exposed to 50 µg/cm^2 MWCNT or crocidolite for 0, 6, and 18 h. A, After the treatments, the cells were lysed, and the level of cleaved PARP, full PARP, and Beta-actin were assessed by Western blot analysis as described in *Materials and methods*. (B) Densitometric analysis of Western blots of cleaved PARP signals normalized to full PARP. The fold activations are relative to normalized values of unstimulated control cells. The presented values are the mean of three experiments.

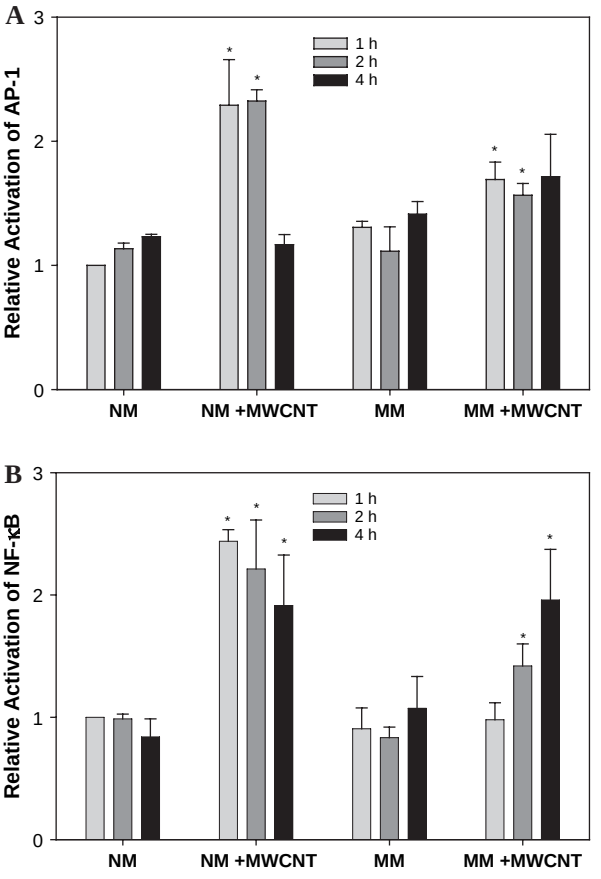

Figure 10. Effect of MWCNT on the activation of AP-1 (A), and NF-κB (B) in NM and MM cells. The cells were treated with dispersion vehicle (control) or 25 µg/cm^2 of MWCNT for 1, 2, or 4 h. Activation of AP-1 and NF-κB in nuclear extractions was determined by ELISA. *Indicates a significant increase from control ($p < 0.05$).

several micrometers. These MWCNT have a high aspect ratio and bio-durability that are characteristic features of amphibole asbestos and may behave like asbestos (Takagi et al. 2008). This potential biologic response on the induction of mesothelioma was recently reported in a study by the intraperitoneal administration of large doses of MWCNT in p53 heterozygous mice (Takagi et al. 2008). It was also reported that MWCNT caused a proinflammatory response induced by ROS generation and was found to be localized within human epidermal keratinocytes (Monteiro-Riviere et al. 2005). *In vivo* intratracheally administered MWCNT in rats showed lung persistence, inflammation and fibrosis stimulated by TNF-α production (Muller et al. 2005). These authors also reported that significant fractions of MWCNT and ground MWCNT still remained in the rat lung even after 60 days (80% and 40%, respectively, of the highest and lowest doses administered). These results suggest that MWCNT may have potential toxic effects on the respiratory tract, and their length appears to modulate lung clearance kinetics (Muller et al. 2005). Whether MWCNT translocate to the pleura and/or extrapulmonary locations is still to be elucidated and merits further investigation. Bio-persistence of an inhaled particle within the lung often determines its toxicity (Oberdörster 2002). Extensive research over the past decades has shown that the indestructible, biopersistent asbestos fibers with enhanced persistent ability to generate ROS can activate signaling of many molecular events that are important contributing factors in the development of mesothelioma.

Since oxidant-dependent and independent mechanisms are involved in the development of mesothelioma, we investigated in this study several mechanistic events that are likely involved in the development of mesothelioma. Although intrinsic ability to generate ROS by the MWCNT is limited due to the low level of catalytic iron present, the cellular uptake and relentless generation of ROS by the bio-persistent fibers is likely be the major factor involved in the signaling of several molecular cascades of events reported here. To compare some of the major signaling events we also used crocidolite as a benchmark of positive control.

An interaction of particulate matter with biological systems through ROS as a possible mechanism involved in cell toxicity has been proposed (Xia et al.

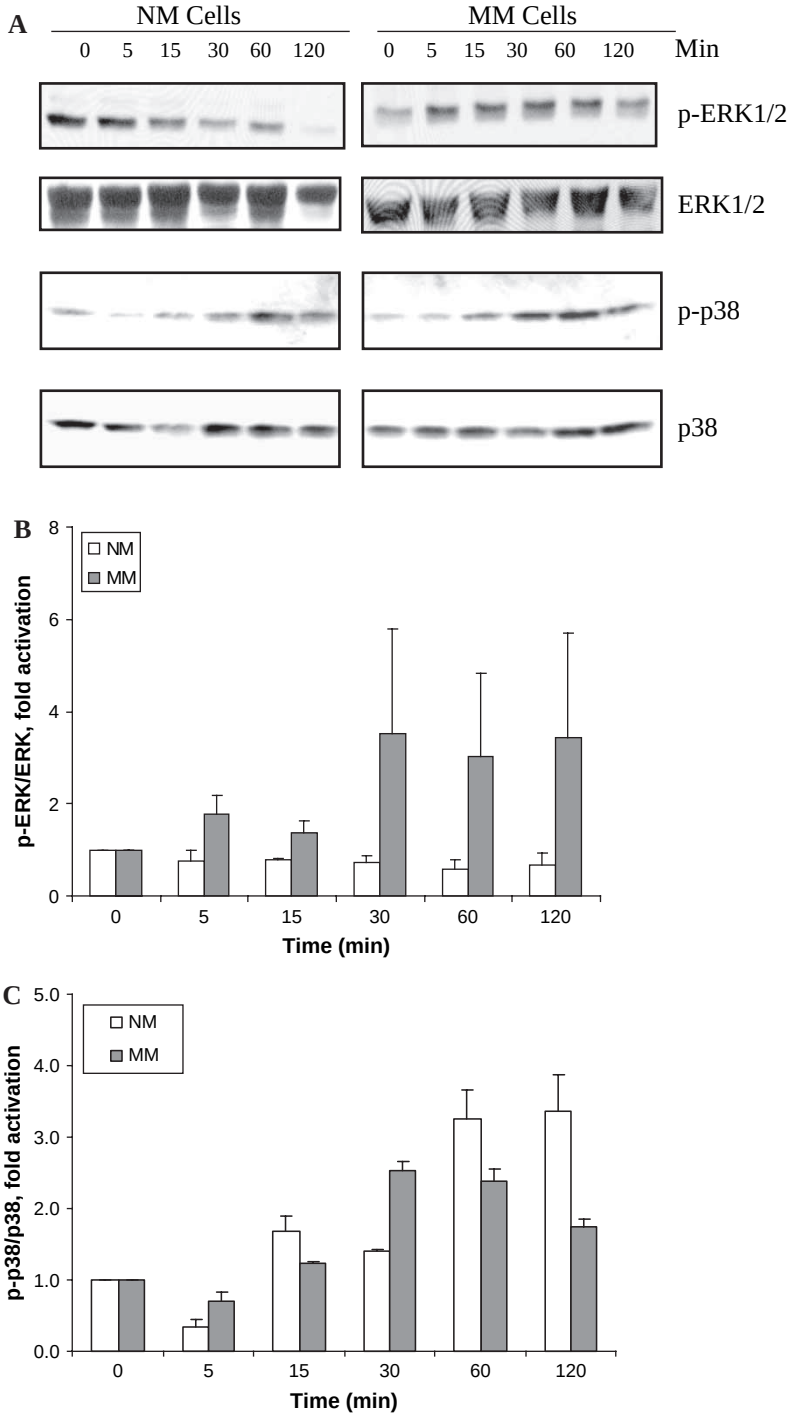

Figure 11. Effect of MWCNT on the activation of MAPKs in NM and MM cells. (A) Western blot analysis of NM and MM cells treated with vehicle or 25 μg/cm^2 MWCNT for 5–120 min. The cells were lysed, and phospho-specific and nonphospho-specific antibodies against phosphorylated and non-phosphorylated ERKs and p38 were assayed using PhosphoPlus MAPKs kit. The phsosphorylated and nonphosphorylated proteins were analyzed using the same transferred membrane following a stripping procedure. (B) Densitometric analysis of Western blots of p-ERK1/2 signal normalized to total-ERK1/2. (C) Densitometric analysis of Western blots of p-p38 signal normalized to total p38. The fold activations are relative to normalized values of unstimulated cells. The results presented are the mean ± SEM of three experiments.

2006). Furthermore, excessive generation of ROS usually leads to an imbalance between oxidant and antioxidant mechanism, which is manifested through oxidative stress. When the balance is in the favor of ROS production, it can interact or modify cellular proteins, lipids, and DNA. The

oxidative stress-induced assault could lead to cellular and molecular events including cell death via an apoptotic pathway or necrosis (Lee et al. 1997; Higuchi 2004; Takahashi et al. 2004). In the present study, minimal ROS was detected following exposure of cells to MWCNT containing low levels of iron. Therefore, as an inducer of radicals, MWCNT are less potent than asbestos and the primary factors in determining toxicity/carcinogenicity may be associated with its fibrous morphological feature. Even though, MWCNT generated little radical species, we show that exposure of both cell types to MWCNT resulted in cell toxicity manifested through decrease of cell viability, release of LDH, increased apoptosis, increased DNA damage, activation of γ-H2AX, and PARP, indicators of cyto- and genotoxicity. Similar results were observed for crocidolite exposure, although the potency of crocidolite was higher for some end-points.

If the MWCNTs remain bio-persistent, continued cellular oxidative stress may result which can lead to impairment of DNA repair mechanism resulting in DNA mutations, change of growth pattern, gene expression, and cell transformation. These events are recapitulated in animal models exposed to asbestos during the development of malignant mesothelioma (Vaslet et al. 2002; Altomare et al. 2005).

AP-1 has been identified as a target of the MAPK family, including ERKs, JNKs, and p38 kinase (Karin et al. 1997). In addition, it has been suggested that the activation of NF-κB is regulated by some upstream MAPK that regulate JNK activation in the cells (Aggarwal & Natarajan 1996). Increased expression and transactivation of *jun* and *fos* proto-oncogene family, the members of AP-1 transcription factor, in response to pathogenic particles such as silica, and crocidolite asbestos is well documented *in vitro* and *in vivo* studies (Heintz et al. 1993; Shukla et al. 2001). Both *c-fos* and *c-jun* are 'immediate-early response' genes, and their transcription is rapidly induced independently of the *de novo* protein synthesis following cell stimulation (Su & Karin 1996). Conversely, NF-κB has been implicated as one of the most important factor in the regulation of inflammation and increased cell survival, events that may govern proliferative responses after stress (Poynter et al. 2004). NF-κB is a ubiquitous transcription factor that can be activated by ROS, cytokines, growth factors, bacteria, viruses, UV irradiation, airborne particulate matter, and inorganic minerals such as asbestos or silica (Haegens et al. 2007). In the present study, NM and MM cells exposed to MWCNT (25 μg/cm^2) resulted in the early transactivation of AP-1 and NF-κB. These results suggest a biological effect of MWCNT associated with cell injury. The upregulation of these molecular changes in mesothelial cells may be important in promoting carcinogenesis. The activation/transactivation of several transcription factors is regulated by MAPK pathways. The transcription factor AP-1 has been identified as a target of the MAPK family, including ERKs, JNK, and p38 kinase (Karin 1995). NF-κB is also an inducible transcription factor that mediates signal transduction between cytoplasm and nucleus in many cell types (Baeuerle & Henkel 1994). Among MAPKs family members, p38 kinase had been shown to stimulate NF-κB in rabbit articular chondrocytes (Wang et al. 2007). It is evident from the results presented here that the ERK1/2 or the p38 are significantly activated by MWCNT in NM and MM cells in a time-dependent manner, and the activation seem to be cell type specific. The mechanism by which AP-1 and NF-κB are activated/transactivated in the present study is perhaps through the MAPKs, the ERK1/2 or the p38. In NM cells only p38 was activated by MWCNT, while in MM cells the EKR1/2 and p38 were activated. Similarly, in the present study both transcription factors AP-1 and NF-κB were activated in response to stimulation with MWCNT. The contribution of ERK1/2 and p38 in the activation/transactivation of these transcription factors, AP-1 and NF-κB, in response to diverse extracellular stimuli is well documented. This may modulate the expression of *c-fos*, *c-jun,* and *c-mic* to induce cell proliferation, apoptosis, and other events important in carcinogenesis.

Although in the present study we report a low level of ROS, indeed we find that MWCNT induce DNA damage, activate γ-H2AX and induce the transactivation of AP-1 and NF-κB. γ-H2AX is a component of DNA repair mechanism that is activated when DNA double-strand break occur. Also, we find that MWCNT increase the level of cleaved PARP-1. PARP-1 is a DNA-binding protein that is primarily activated by nicks in DNA and regulates the activity of various enzymes that are involved in the control of DNA metabolism (Genovese & Cuzzorcrea 2008). However, the effect of MWCNT on PARP was lower compared to crocidolite effect in both cell types. Also, we observed, differential cellular responses to MWCNT and crocidolite in both cell lines indicative of molecular or genetic differences in the malignant cells. The exact mechanism by which MWCNT induces cellular reactions is not known yet, however we propose several contributing factors may be involved in inducing toxicity and molecular mechanisms. Perhaps a combination of low level of ROS produced by MWCNT and the persistent interaction of MWCNT by cells may contribute to cellular reactions. MWCNT used in this study is reported to have 0.27% iron which may not be all present on the surface for biological interaction since some may be

within the core of the tube. Similarly, the exact mechanism by which asbestos fibers induce mesothelial cell injury to cause mesothelioma is not clear, but amphibole asbestos containing a significantly greater amount of iron with the enhanced potential to generate ROS produce disease only after several years of latency (Mossman et al. 1996; Vallyathan & Shi 1997; Kamp & Weitzman 1999).

In conclusion, the present study shows that MWCNT upon interaction with normal and malignant mesothelial cells elicit toxic effect and induce several molecular changes that have been associated with carcinogenesis. Exposure of mesothelial cells to MWCNT containing significantly lower levels of iron resulted in cell death, cytotoxicity, and DNA damage. Furthermore, this study shows that MWCNT have the potential to activate important molecular signaling factors that are associated with cellular transformation.

***Declaration of interest*:** The authors report no conflicts of interest. The authors alone are responsible for the content and writing of the paper. The findings and conclusions in this report are those of the authors and do not necessarily represent the views of the National Institute for Occupational Safety and Health.

References

Aggarwal BB, Natarajan K. 1996. Tumor necrosis factors: Developments during the last decade. Eur Cytokine Network 7:93–124.

Altomare DA, Valset CA, Skele KL, De Rienzo A, Devarajan K, Jhanwar SC, McClatchey AI, Kane AB, Testa JR. 2005. A mouse model recapitulating molecular features of human mesothelioma. Cancer Res 65:8090–8095.

Baeuerle PA, Henkel T. 1994. Function and activation of NF-kappa B in the immune system. Annu Rev Immunol 12: 141–179.

Bang JJ, Guerrero PA, Lopez DA, Murr LE, Esquivel EV. 2004. Carbon nanotubes and other fullerene nanocrystals in domestic propane and natural gas combustion streams. J Nanosci Nanotechol 4:716–718.

Brunauer S, Emmett PH, Teller E. 1938. Adsorption of gases in multimolecular layers. A Am Chem Soc 60:309–319.

Chen J, Shan JY, Tsukada T, Munekane F, Kuno A, Matsuo M, Hayashi T, Kim YA, Endo M. 2007. The structural evolution of thin multi-walled carbon nanotubes during isothermal annealing. Carbon 45:274–280.

Cowell IG, Sunter NJ, Singh PB, Austin CA, Durkacz BW, Tilby MJ. 2007. γH2AX foci form preferentially in euchromatin after ionizing radiation. PLoS ONE 10:e1057.

Craighead H, Leong K. 2000. Applications: Biotechnology, medicine, and healthcare. In: Roco MC, Williams RS, Alivisatos P, editors. Nanotechnology research directions: IWGN workshop report. Vision for nanotechnology research and development in the next decade. US National Science and Technology Council, Washington, DC, (also Boston: Kluwer Academic Publishers. pp 107–120).

Ding M, Dong Z, Chen F, Pack D, Ma WY. 1999. Asbestos induces activator protein-1 transactivation in transgenic mice. Cancer Res 59:884–889.

Donaldson K, Aitken R, Tran L, Stone V, Duffin R, Forrest G, Alexander A. 2006. Carbon natotubes: A review of their properties in relation to pulmonary toxicology in workplace safety. Toxic Sci 92:5–22.

Endo M, Hayashi T, Kim YA, Terrones M, Dresselhaus MS. 2004. Applications of carbon nanotubes in the 21st century. Philos Transact A Math Phys Eng Sci 362:2223–2238.

Genovese T, Cuzzorcrea S. 2008. Role of free radicals and poly(ADP-ribose)polymerase-1 in the development of spinal cord injury: New potential therapeutic targets. Curr Med Chem 15:477–487.

Gwinn M, Vallyathan V. 2006. Nanoparticles: health effects – pros and cons. Environ Health Perspect 114:1818–1825.

Haegens A, Barret TF, Gell J, Shukla A, MacPherson M, Vacek P, Pounter ME, Butnor KJ, Janssen-Heininger YM, Steele C, Mossman BT. 2007. Airway epithelial NF-?B activation modulates asbestos-induced inflammation and mucin production *in vivo*. J Immunol 178:1800–1808.

Heintz NH, Janssen YMW, Mossman BT. 1993. Persistent induction of c-fos and c-jun expression by asbestos. Proc Natl Acad Sci USA 90:3299–3303.

Higuchi Y. 2004. Glutathione depletion-induced chromosomal DNA fragmentation associated with apoptosis and necrosis. Cell Mol Med 8:455–464.

Holman MW, Lackner DI. 2006. The nanotech report. 4th ed. New York: Lux Research Inc.

Huo P-X, Xu S-T, Ying Z, Yang Q-H, Liu C, Cheng H-M. 2003. Hydrogen adsorption/desorption behavior of multi-walled carbon nanotubes with different diameters. Carbon 41: 2471–2476.

Kam NSW, Jessop TC, Wender PA, Dai H. 2004. Nanotube molecular transporters: Internalization of carbon nanotube-protein conjugates into mammalian cells. J Am Chem Soc 126:6850–6851.

Kamp DW, Weitzman SA. 1999. The molecular basis of asbestos induced lung injury. Thorax 54:638–682.

Karin M. 1995. The regulation of AP-1 by mitogen-activated protein kinase. J Biol Chem 270:16843–16846.

Karin M, Liu Z, Zandi E. 1997. AP-1 function and regulation. Curr Opin Cell Biol 9:240–246.

Kim YA, Hayashi TT, Endo M, Kaburagi T, Tsukada T, Shan JY, Osata K, Tsuruoka S. 2005. Synthesis and structural characterization of thin multi-walled carbon nanotubes with a partially facetted cross section by a floating reactant method. Carbon 43:2243–2250.

Koyama S, Endo M, Kim YA, Hayashi T, Yanagisawa T, Osaka K, Koyama H, Haniu H, Kuroiwa N. 2006. Role of systemic T-cells and histopathological aspects after subcutaneous implantation of various carbon nanotubes in mice. Carbon 44: 1079–1092.

Lam CW, James JT, McCluskey R, Arepalli S, Hunter RL. 2006. A review of carbon nanotube toxicity and assessment of potential occupational and environmental health risks. Crit Rev Toxicol 36:189–217.

Lam CW, James JT, McCluskey R, Hunter RL. 2004. Pulmonary toxicity of single-wall carbon nanotubes in mice 7 and 90 days after intratrachael instillation. Toxicol Sci 77:126–134.

Lee FS, Hagler J, Chen ZJ, Maniatis T. 1997. Activation of the IkappaB alpha kinase complex by MEKK1, a kinase of the JNK pathway. Cell 88:213–222.

Leonard SS, Xia C, Jiang BH, Stinefelt B, Klandorf H, Harris GK, Shi X. 2003. Resveratrol scavenges reactive oxygen species and effects radical-induced cellular responses. Biochem Biophys Res Commun 309:1017–1026.

Li Z, Hulderman T, Salmen R, Chapman R, Leonard SS, Young SH, Shvedova AA, Luster MI, Simeonova PP. 2006. Cardiovascular effects of pulmonary exposure to single-wall carbon nanotubes. Environ Health Perspect 115:377–382.

Luo H, Shi Z, Li N, Gu Z, Zhuang Q. 2001. Investigation of the electrochemical and electrocatalytic behavior of single-wall carbon nanotube film on a glassy carbon electrode. Anal Chem 73:915–920.

Manna SK, Sarkar S, Barr J, Wise K, Barrera EV, Jejelowo O, Rice-Ficht AC, Ramesh GT. 2005. Single-walled carbon nanotube induces oxidative stress and activates nuclear transcription factor-kappaB in human keratinocytes. Nano Lett 5:1676–1684.

Maynard AD. 2007. Nanotechnology: The next big thing, or much ado about nothing? Ann Occup Hyg 51:1–12.

Maynard AD, Baron AP, Foley M, Shvedova AA, Kisin ER, Castranova V. 2004. Exposure to carbon nanotube material: Aerosol release during the handling of unrefined single-walled carbon nanotube material. J Toxicol Environ Health Part A 67:87–107.

Mercer RR, Scabilloni JF, Wang L, Kisin E, Murray AR, Schwegler-Berry D, Shvedova AA, Castranova V. 2008. Alteration of deposition pattern and pulmonary response as a result of improved dispersion of aspirated single walled carbon nanotubes in a mouse model. Am J Physiol Lung Cell Mol Physio 294:L87–97.

Monteiro-Riviere NA, Nemanich RJ, Inman AO, Wang YY, Riviere JE. 2005. Multi-walled carbon nanotubes interactions with human epidermal keratinocytes. Toxicol Lett 155: 377–384.

Mossman BT, Kamp DW, Weitzman SA. 1996. Mechanisms of carcinogenesis and clinical features of asbestos-associated cancers. Cancer Invest 14:466–480.

Muller J, Huaux F, Moreau N, Misson P, Heilier, JF, Delos M, Arras M, Fonseca A, Nagy JB, Lison D. 2005. Respiratory toxicity of multi-wall carbon nanotubes. Toxicol Appl Pharmacol 207:221–231.

Murr LE, Bang JJ, Esquivel EV, Guerrero PA, Lopez DA. 2004a. Carbon nanotubes, nanocrystal forms and complex nanoparticle aggregates in common fuel-gas combustion source and ambient air. J Nanoparticle Res 5:1–11.

Murr LE, Bang JJ, Lopez DA, Guerrero PA, Esquivel EV, Choudhuri AR, Subramanya M, Morandi M, Holian A. 2004b. Carbon nanotubes and nanocrystals in methane combustion and the environmental implications. J Mater Sci 39:2199.

NMAM. 1994. NIOSH 7500 Manual of Analytical Methods. 4th ed.

Oberdörster G. 2001. Pulmonary effects of inhaled ultrafine particles. Int Arch Occup Environ Health 74:1–8.

Oberdörster G. 2002. Toxicokinetics and effects of fibrous and nonfibrous particles. Inhal Toxicol 14:29–56.

Oberdörster G, Oberdörster E, Oberdöster J. 2005. Nanotoxicology: An emerging discipline evolving from studies of ultrafine particles. Environ Health. Perspect 113:823–839.

Pantarotto D, Briand JP, Prato M, Bianco M. 2004. Translocation of bioactive peptides across cell membranes by carbon nanotubes. Chem Commun 1:16–17.

Poland CA, Duffin R, Kinloch I, Maynard A, Wallace WAH, Seaton A, Stone V, Brown S, MacNee W, Donaldson K. 2008. Carbon nanotubes introduced into the abdominal cavity of mice show asbestos-like pathogenicity in a pilot study. Nature Nanotech 3:423–428.

Poynter ME, Cloots R, van Woerkom T, Butnor KJ, Vacek P, Taatjes DJ, Irvin CG, Janssen-Heininger YM. 2004. NF-B activation in airways modulates allergic inflammation but not hyperresponsiveness. J Immunol 173:7003–7009.

Shukla A, Timblin CR, Hubbard AK, Bravman J, Mossman BT. 2001. Silica-induced activation of c-Jun-NH2-terminal amino kinases, protracted expression of the Activator Protein-1 proto-oncogene, fra-1, and S-phase alterations are mediated via oxidative stress. Cancer Res 61:1791–1795.

Shvedova AA, Castranova V, Kisin ER, Schwegler-Berry D, Murray AR, Gandelsman VZ, Maynard AD, Baron P. 2003. Exposure to carbon nanotube material: assessment of nanotube cytotoxicity using human keratinocyte cells. J Toxicol Environ Health Part A 66:1909–1926.

Shvedova AA, Kisin ER, Mercer RR, Murray SR, Johnson AJ, Potapovich AI, Tyurina YY, Gorelik O, Arepalli S, Schwegler-Berry D, et al. 2005. Unusual inflammatory and fibrogenic pulmonary responses to single-walled carbon nanotubes in mice. Am J Physiol Lung Cell Mol Physiol 289:L698–708.

Su B, Karin M. 1996. Mitogen-activated protein kinase cascades and regulation of gene expression. Curr Op Immunol 8: 402–411.

Takagi A, Hirose A, Nishimura T, Fukumori N, Ogata A, Ohashi N, Kitajima S, Kanno J. 2008. Induction of mesothelioma in p53+/−mouse by intraperitoneal application of multi-wall carbon nanotube. J Toxicol Sci 33:105–116.

Takahashi A, Masuda A, Sun M, Centonze VE, Herman B. 2004. Oxidative stress-induced apoptosis is associated with alterations in mitochondrial caspase activity and Bcl-2-dependent alterations in mitochondrial pH (pHm). Brain Res Bull 62:497–504.

Vallyathan V, Shi X. 1997. The role of oxygen free radicals in occupational and environmental lung diseases. Environ Health Perspect 105:165–177.

Vaslet CA, Messier NJ, Kane AB. 2002. Accelerated progression of asbestos-induced mesotheliomas in heterozygous p53+/− mice. Toxicol Sci 68:331–338.

Wang H, Wang Z, Chen J, Wu J. 2007. NO Apoptosis induced by NO via phosphorylation of p38 MAPK that stimulates NF-(B, p53 and caspase-3 activation in rabbit articular chondrocytes. Cell Bio Intern 31:1027–1035.

Warheit BR, Laurence KL, Reed DH, Roach GAM, Reynolds, Webb TR. 2004. Comparative pulmonary toxicity assessment of single-wall carbon nanotubes in rats. Toxicol Sci 77: 117–125.

Xia T, Kovochich M, Nel A. 2006. The role of reactive oxygen species and oxidative stress in mediating particulate matter injury. Clin Occup Environ Med 5:747–898.